Turbulence, Heat and Mass Transfer 6
K. Hanjalić, Y. Nagano and S. Jakirlić (Editors)

Drag Reduction for Trucks by Active Flow Control of the Wake Behind the Trailer

M. El-Alti[1], P. Kjellgren[1,2] and L. Davidson[1]

[1]*Division of Fluid Dynamics, Department of Applied Mechanics, Chalmers University of Technology, Göteborg , Sweden, mohammad.el-alti@chalmers.se*

[2]*Per Kjellgren Engineering, Nyvollhagen 9, 4070 Randaberg, Norway*

Abstract — Several hundred large-eddy simulations with active flow control have been carried out to propose a novel rear end of a trailer. It is found that a reduction of aerodynamic drag by up to 25% or more is achieved for certain configurations. The reduction is mainly the result of a pressure recovery on the flap surface and the rear end of the trailer. The parameters of the novel rear end geometry and the variables of AFC are investigated. A thorough analysis of the mechanism of flow control and the flow characteristics of the forced and unforced case is reported.

1. Introduction

1.1. Background

The aerodynamics of today's trucks is far from optimal. While manufacturers of personal cars develop their sophisticated models that are designed for low fuel consumption, the rear end of all trucks is in principle squared, with four perpendicular corners. Truck manufacturers around the world have begun to realize the great need that exists to reduce fuel consumption and improve the environmental performance of trucks. In order to develop more environmentally friendly vehicles to meet the growing environmental requirements, the harder international competition in the heavy vehicle industry and the still increasing fuel prices, the trailer must be considered and included in the aerodynamic design development [1] and advanced active flow control techniques must be implemented.

Most of the drag on a truck is caused by the wake behind the trailer. This is introduced by the sharp edges on the rear end where the flow naturally separates. This effect gives rise to a large low pressure region and thus increases the pressure difference between the front and back. The large low pressure region acts as a force that sucks the whole truck backwards. An effective way to increase the pressure on the back is by introducing angled flaps. By introducing the flaps at an angle less than the natural separation angle, the wake becomes narrower, which decreases the base drag. If the angle is increased, the drag increases. The idea is now to further decrease the drag by attaching the flow onto the flap surface again. The attachment process is done using active flow control (AFC). The idea of using flaps and reattaching the separated flow is in line with research that has shown successful results on tilt-rotor aircraft done by the present authors in [2, 3], which was a continuation of previous research [4, 5].

The achievement of two main flow physical goals is expected from this technique. The first is to narrow the size of the wake by attaching the separated flow, and the second is to make the wake less intensive. The former is achieved by the introduction of flaps at a high angle at the rear end and reattaching the naturally separated flow onto the flap surface. The reattachment

process occurs by the increased level of turbulence close to the separation point, which re-energizes the weak boundary layer, that is to separate. The latter is achieved by the creation of small vortices that are generated by the blowing and suction of the AFC and whose intensity increases downstream. These vortices develop a shear layer that destroys the dissipative wake structure and makes the wake less intensive.

VOLVO 3P and SKAB will in the near future manufacture a prototype configuration and make a full-scale test of a truck with the optimal AFC configuration. The actuator that will be used is a simple synthetic jet actuator [6]. The use of AFC requires effective actuators that are capable of producing enough momentum and still have a low energy consumption. The net drag reduction, or the efficiency of the AFC, is then defined by

$$\eta_{AFC} = 1 - \frac{P_a}{P_s} \tag{1}$$

where P_a is the power required to generate the actuation and P_s is the power saved through drag reduction due to AFC. The present efficiency, η_{AFC}, is at least 80%. The net drag reduction will thus be

$$\Delta C_{D,net} = \eta_{AFC} \Delta C_{D,AFC} \tag{2}$$

More details about the project, the optimization procedure using response surface methodology and the uncertainty analysis are found in [7].

1.2. Other efforts

Several studies have been carried out to minimize the drag on trucks, both purely passive investigations and investigations that have combined active flow control strategies. The investigations in [8] and [9] both used passive devices mounted at the rear end of the trailer. In [8] a drag reduction of 15% was reached by using base flaps inclined at $15°$. Attempts were made in [9] with vortex generators, base flaps and boat tail. The vortex generators actually increased the drag while the flaps and boat tail showed marginal drag reduction.

Several active flow control efforts have been made, both with and without flaps. Investigations were made without flaps in [10] and [11], where the authors in [10] used a circular cylinder that had a built-in actuator and reached a drag reduction of 20%. In [11] they used closed-loop control on a blunt trailing edge and reached a 10% drag reduction. One successful effort is reported in [12], where a drag reduction of about 30% was achieved using steady blowing. These are promising results, but the use of steady blowing is energy consuming and the net drag reduction is not that high.

Bearing these efforts in mind, we made a thorough parameter study using periodic blowing, which is much more effective than steady blowing. The authors in [13] compared steady blowing versus periodic blowing superimposed with small amount of steady blowing to delay the separation on a wing surface in order to enhance the lift and decrease the drag. The periodic blowing required much lower power compared to steady blowng and showed comparable end results.

2. Numerical Method

2.1. Large-eddy simulation

The flow behind the truck is unsteady, and the pulsating (i.e. oscillating) jets are used as forcing. Thus the modeling strategy must be transient. The modeled actuator is very narrow, and the excitation velocity is about 80% of the free stream velocity. The actuation frequency is also

much higher than the Strouhal frequency, and thus fine resolution is needed both in space and time. Large-eddy simulation is thus used in order to make accurate prediction of the turbulent flow as it provides both instantaneous field data and high accuracy. The Reynolds number is $200,000$, which is in the range of manageable LES. A higher Reynolds number, such as in full-scale flow, would have forced us to use a hybrid LES/RANS approach, such as DES. The commercial FlowPhys ver. 2.0 software was used for the computations in this work. It has a semi-implicit, fractional step finite element solver.

The filtered Navier-Stokes equations read

$$\frac{\partial \bar{u}_i}{\partial t} + \frac{\partial}{\partial x_j}\left(\bar{u}_i \bar{u}_j\right) = -\frac{1}{\rho}\frac{\partial \bar{p}}{\partial x_i} + \nu \frac{\partial^2 \bar{u}_i}{\partial x_j \partial x_j} - \frac{\partial \tau_{ij}}{\partial x_j} \tag{3}$$

where $\tau_{ij} = \overline{u_i u_j} - \bar{u}_i \bar{u}_i$ is the sub-grid scale stresses modeled as

$$\tau_{ij} - 1/3\delta_{ij}\tau_{kk} = -2\nu_{sgs}\bar{s}_{ij} \tag{4}$$

where ν_{sgs} is

$$\nu_{sgs} = (C_S f \Delta)^2 \sqrt{2\bar{s}_{ij}\bar{s}_{ij}} \tag{5}$$

and $\bar{s}_{ij}$ is

$$\bar{s}_{ij} = 1/2\left(\frac{\partial \bar{u}_j}{\partial x_j} + \frac{\partial \bar{u}_j}{\partial x_i}\right) \tag{6}$$

The Smagorinsky model (eq. 4) for the sub-grid scales is used with the Smagorinsky constant $C_S = 0.20$. In the near-wall region ($20\ cm$), the filter width is reduced using the Van Driest damping function.

$$f = 1 - e^{-y^+/A^+} \tag{7}$$

where $A^+ = 25$ and y^+ is calculated by searching for the closest distance between a node in the domain and the wall node. The temporal discretization is the explicit four-step Runge-Kutta scheme for the convection terms and the Crank-Nicholson method for the diffusion terms. The spatial discretization scheme is the pure central difference (CD). The time step size was controlled by an adaptive time stepper that kept the max Courant number equal to two. The check was done every 10th time step. The number of time steps was typically between $100\,000$ and $200\,000$, and the size of the time step varied between 10^{-4} and $6 \cdot 10^{-5}$. The forcing is modeled as a transient velocity inlet, and the governing variables are the slot width, the velocity (both magnitude and direction) and the frequency. The RMS momentum from the slot is defined as

$$J_{rms} = \int \rho u_{rms}^2 \, dh = \rho u_{rms}^2 \Delta h \tag{8}$$

Δh is the effective slot width. Further, we define the momentum-coefficient as

$$C_{\mu\, rms} = \frac{J_{rms}}{w\frac{1}{2}\rho u_\infty^2} = \frac{u_{rms}^2 \Delta h}{w\frac{1}{2}u_\infty^2} \tag{9}$$

where w is the width of the truck. The velocity in the slot is given from eq. 9 by

$$u_{rms} = \sqrt{\frac{C_{\mu\, rms}\ w\ u_\infty^2}{2\Delta h}} \tag{10}$$

We further assume that the forcing is purely sinusoidal, i.e.

$$u(t) = \sqrt{2} u_{rms} \sin(2\pi F t) \tag{11}$$

Finally, we define the non-dimensional forcing frequency as

$$F^{+} = \frac{F \cdot X_{TE}}{U_{\infty}} \tag{12}$$

where X_{TE} is the distance from the slot to the trailing edge of the flap.

2.2. Computational domain

We use a simplified truck model in our simulations. The truck is simplified as a rectangular bluff body with typical width ($w = 2.6\ m$) and length ($l = 13.0\ m$) relevant for a real truck and assuming periodicity in the third direction (height), i.e. the domain is three-dimensional (figure 1(a)). The truck is mounted with angled flaps on the rear end in which the oscillating synthetic jet actuators are placed (figure 1(b)). The actuators are modeled as a time varying boundary condition (slot). The slot extends over the entire height (z) of the truck.

The truck geometry is shown in figure 1(a) and 1(b). The inlet flow is modeled as an inlet boundary condition (BC) with a prescribed constant free stream velocity, $U_{\infty} = 25\ m/s$. The Reynolds number is reduced to 200 000 by increasing the viscosity to $\mu = 3.25 \cdot 10^{-4}$ and the density was set to $\rho = 1.0$. The outlet BC is the standard outlet with a zero gradient. The side walls are prescribed to be frictionless walls, i.e. slip BC.

The computational mesh is shown in figure 2. The number of nodes in the wake and the flap region is very large compared to that in the free stream region. The mesh size is about $1.4 - 3.3$ million nodes and consists of unstructured quad elements in the $x - y$ plane and structured quad elements in the span-wise direction. The quality of the mesh was very high close to the wall and in the flap region. At the end of the side walls of the truck (prior to the flap), max $y^{+} < 2$, mean $y^{+} \sim 1$, max $\Delta x^{+} < 30$, mean $\Delta x^{+} \sim 20$, max $\Delta z^{+} \sim 130$, mean $\Delta z^{+} \sim 100$ for low resolution, and max $\Delta z^{+} \sim 60$ and mean $\Delta z^{+} \sim 50$ for high resolution. A thorough dependence study of spanwise mesh resolution and domain size is reported in [7].

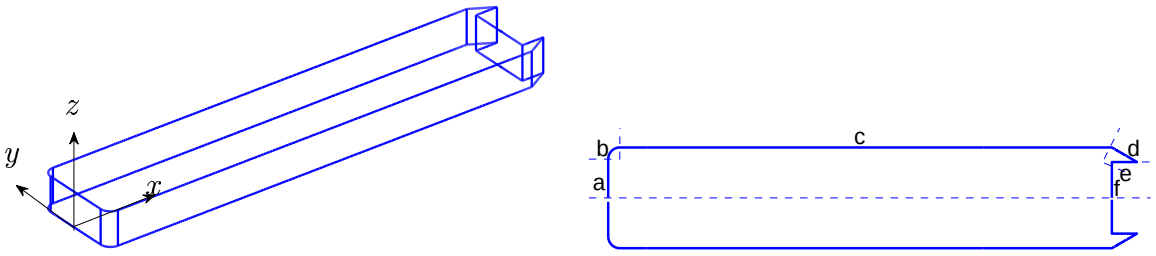

(a) Computational domain

(b) Line representation

Figure 1: (a) Simplified truck model: inlet at $x = -12w$; outlet at $x = 30w$; slip side walls at $y = -8.5w$ and $y = 8.5w$. (b) Line representation of the truck showing different parts used in the C_P analysis.

3. Results

The following results are a comparison of the unforced and the forced cases. The unforced case is denoted as "AFC OFF" and the forced as "AFC ON". The specific forced case chosen is one that has shown maximal drag reduction compared with the unforced one. The specifications of

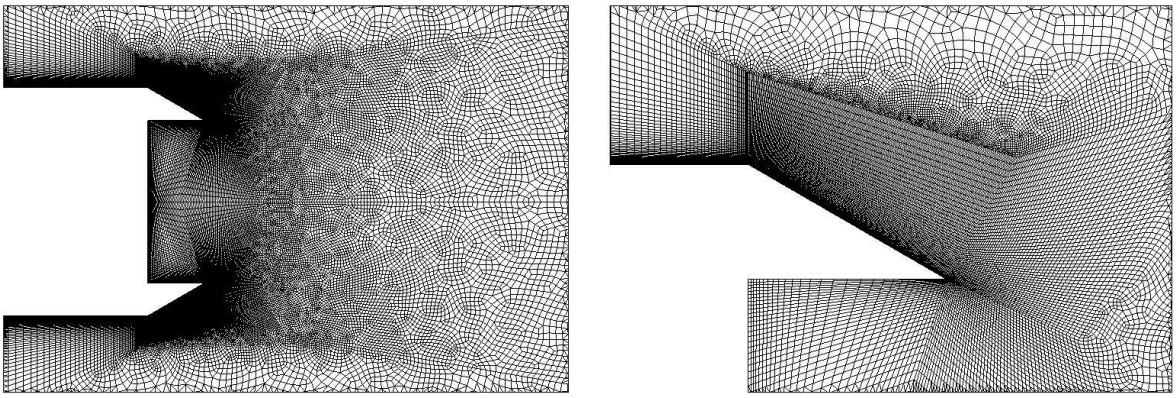

(a) Mesh around the Wake

(b) Mesh around the flap

Figure 2: 2D slice of the proposed novel rear-end of trailer, geometry and mesh.

the chosen case are listed in table 1. The slot width is set to $\Delta h = 6\ cm$, which means that $C_\mu = 1.0\%$ corresponds to $u_{rms} \sim 20\ m/s$, see eq. 10 . The location of the slot is at the upper edge of the flap. The spanwise domain size is $0.4\ m$ with 16 cell layers, which corresponds to max $\Delta z^+ = 130$ and mean $\Delta z^+ = 100$. Both the instantaneous and time averaged quantities are plotted at three regions of interest: a general plot of the whole truck with upstream and downstream regions, a plot of the wake region and finally a plot of the flap region. Only the most interesting are presented here. FL, FA and SA denote flap length, flap angle and slot angle, respectively. SA is defined relative to the flap surface.

Table 1: Specifications of the forced case

AFC parameter	Value
FL	$0.75\ m$
FA	$30\ deg$
SA	$15\ deg$
C_μ	$1.0\ \%$
F^+	0.3

3.1. Instantaneous flow

It is very important to investigate the instantaneous characteristics of the flow in active flow control. We chose to study the instantaneous pressure and velocity streamlines at a specific instant with locally interesting flow features. We expect that the flow for the unforced case is separated from the flap surface because the flap angle is high enough. Furthermore, the separation will develop a strong vortex shedding behind the rear end of the truck. Instantaneously, each vortex developed will manifest itself as a low pressure region moving downstream, as shown in figure 3(a). We also notice the strong high pressure at the front region of the truck and the separated flow at the curvature at the intersection of the front and the sides of the truck, which is evident in both figures 3(a) and 3(b).

In figure 3(a) we can also see that the pressure on the upper flap is low because of the reversed flow in the separation bubble. It is clear that the low pressure region downstream of the flap is suppressed in the forced case. We also notice that a smaller low pressure region is created at the slot location at which the actuation takes place. We can also see that small vortices are created by the actuation, which can be seen at the lower flap in figure 3(b). These small vortices were also noted by [5], who carried out an experiment on flow separation and reattached by AFC on a flap deflected at angles larger than the natural separation angle. The Reynolds number in that study was $Re = 1.65 \cdot 10^5$, which is of same order as in the present work. The separation from the flap surface is also shown in figure 4, which plots the instantaneous velocity streamlines. The instantaneous flow is reattached on the flap surface for the forced case (figure 4(b)). Small vortices created by the actuation can be seen at the downstream edge of the upper flap in figure 4(b). Compared to figure 3(b) the location of these vortices has moved further downstream of the flap surface. We conclude that these vortices that are created by the actuation are moving downstream of the flap surface and create a shear layer in the wake region that makes the vortex shedding weaker and prevents interaction between the naturally created shear layers formed at the upper and lower edges. These vortices are furthermore moving downstream in the wake region with a successively increasing size, destroying the low pressure dominant wake structure and yielding pressure recovery. By its blowing and suction the actuation re-energizes the boundary layer that would separate, and interacts with the ambient flow to introduce vortices that roll down the flap surface. When the flow remains reattached to the flap surface, the wake size becomes narrower.

3.2. Time-averaged flow and wake structure

The effect of the actuation was further studied by time-averaged flow quantities. Pressure, velocity streamlines and vorticity were investigated. To study the level of activity in the wake, i.e. the strength of the vortex shedding, the RMS of pressure was also plotted for different regions.

Figure 5 plots the time-averaged pressure. With AFC off, we notice the expected large low pressure region behind the truck caused by the strong vortex shedding. The low pressure region behind the truck is almost completely suppressed by AFC in figure 5(b). Here we also notice the low pressure region on the flap for the unforced case. However, in the forced case, this region is advanced upstream. We conclude that a low pressure region is created by AFC at the slot location that sucks the flow onto the flap surface.

Figure 6 plots the time-averaged streamlines. It is clear that the wake structure is affected in the forced case. The smaller wake structure of the forced case can be seen in figure 6(b). The wake is narrowed and has a shorter distribution in the free stream direction. It is clear that the time-averaged flow is entirely reattached on the flap surface by active flow control. Furthermore, in the unforced case, flow is coming from the back side of the truck, up to the flap surface. In the forced case, this flow is prevented by the reattached streamlines. This is one of the reasons why the interaction of the lower and upper shear layers is prevented.

The time-averaged vorticity is shown in figure 7. We can draw several conclusions: first we recognize the separation region in the unforced case, showing both positive and negative vorticity; we also notice the strong positive vorticity evolving from the end of the flap. The forced case in figure 7(b) shows that the negative vorticity has moved closer to the flap surface and the positive vorticity (i.e. recirculation) been suppressed almost entirely. The negative vorticity in the forced case confirms our previous discussion about the vortices created by the actuation and rolls down the flap surface.

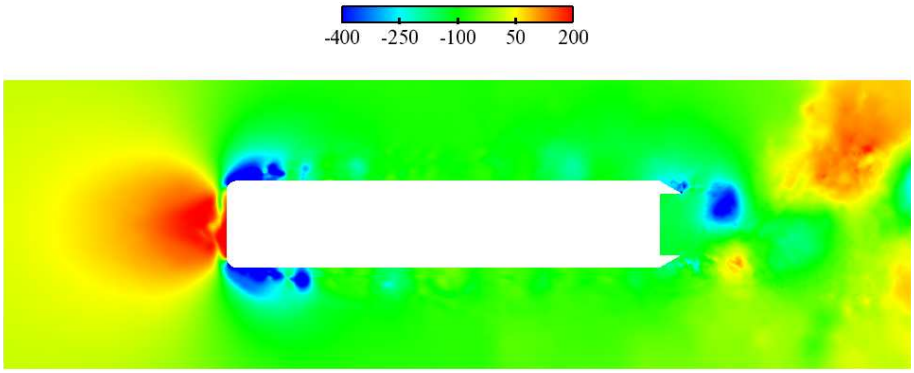

(a) AFC OFF

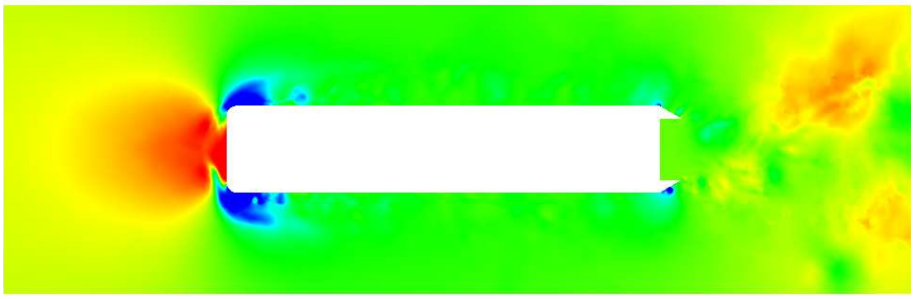

(b) AFC ON

Figure 3: Instantaneous pressure contours. Note the large low pressure region downstream of the upper flap in (a) and how it is suppressed by AFC in (b).

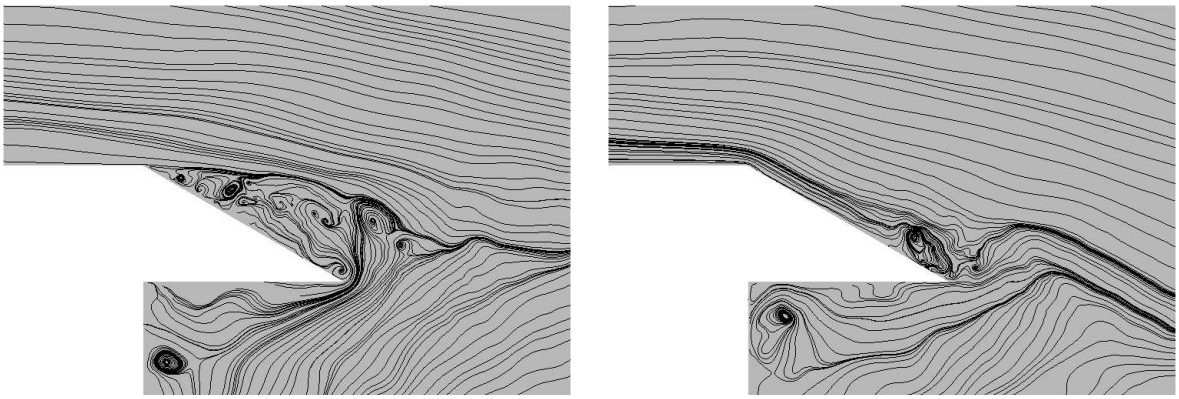

(a) AFC OFF (b) AFC ON

Figure 4: Instantaneous streamlines, zoom around the flap region.

One of the most interesting plots is the RMS of pressure in figure 8. We notice the great suppression of P_{RMS} in the wake region. This causes the wake structure to be less intensive and decreases the level of vortex shedding. At closer look at the flap region, we also conclude

that the actuation is increasing the turbulence on the flap surface in order to reattach the flow. The actuation location itself shows up as increased RMS pressure. The conclusion is that the unforced case is characterized by a highly turbulent and intensive wake while the forced one has a low level of turbulence in the wake, and the forcing makes the wake less intensive and increases the turbulence at the flap surface in order to reattach the flow.

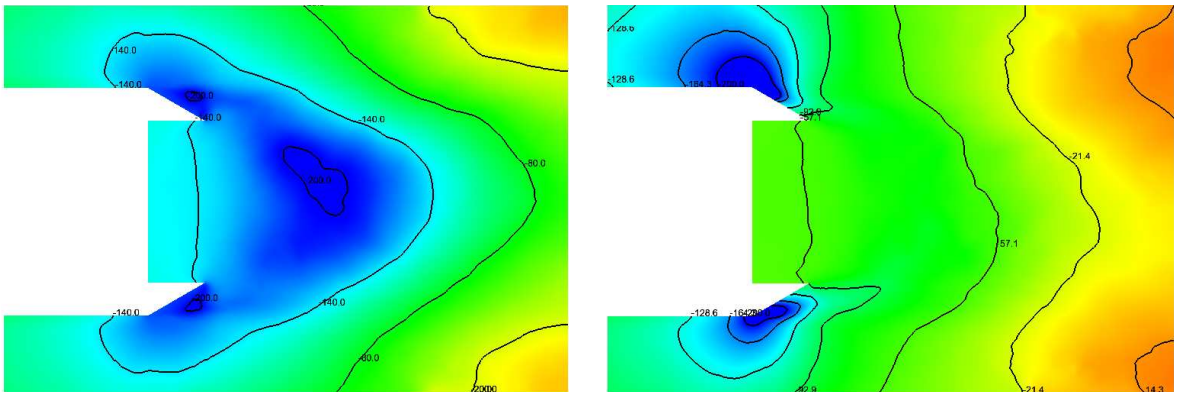

(a) AFC OFF (b) AFC ON

Figure 5: Time-averaged pressure contours, zoom of the wake.

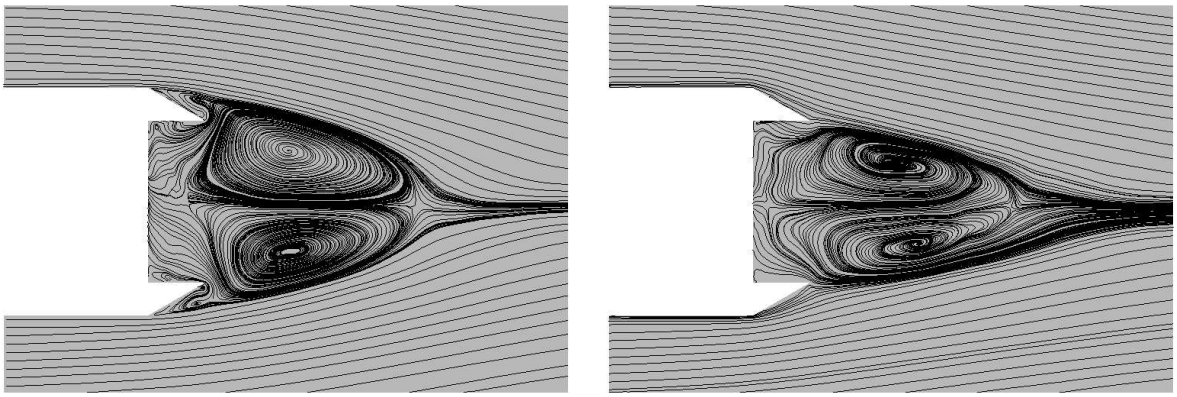

(a) AFC OFF (b) AFC ON

Figure 6: Time-averaged velocity streamlines, zoom of the wake.

3.3. Surface pressure distribution

All letters that indicated location refer to those in figure 1(b). To further study the influence of AFC on the truck body, the surface pressure distribution is plotted in figure 9. We are actually only interested in the projection of the pressure load in the x-direction because this is what contributes to the drag force. As shown in figure 9(b), the impinging location at the symmetry line is almost $C_P = 1$ as expected. The reason for the small discrepancy is mainly that the upstream domain is not large enough. C_P then becomes negative at the curvature, b, and $C_{p,x}$ is exactly zero on the side surface, c. On the flap surface, d, the forced case shows lower C_P

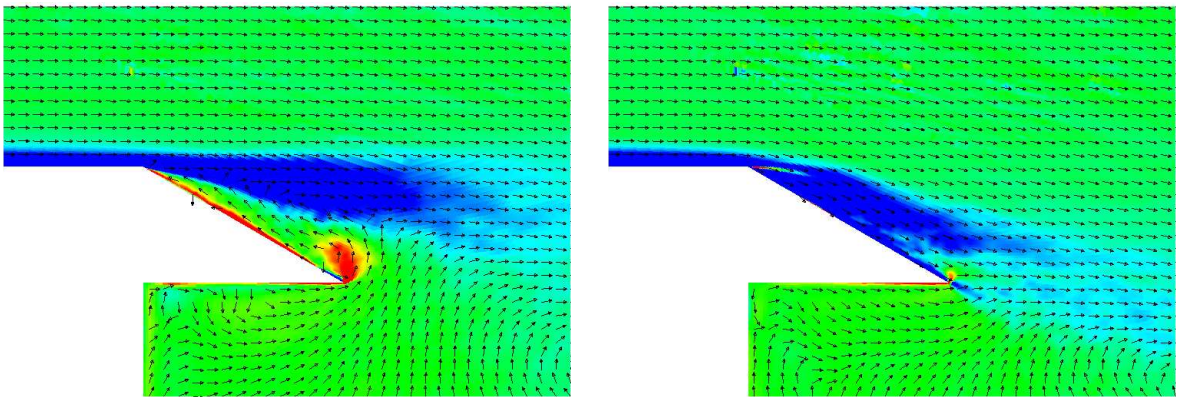

(a) AFC OFF (b) AFC ON

Figure 7: Time-averaged vorticity contours and velocity vectors, zoom around flap region.

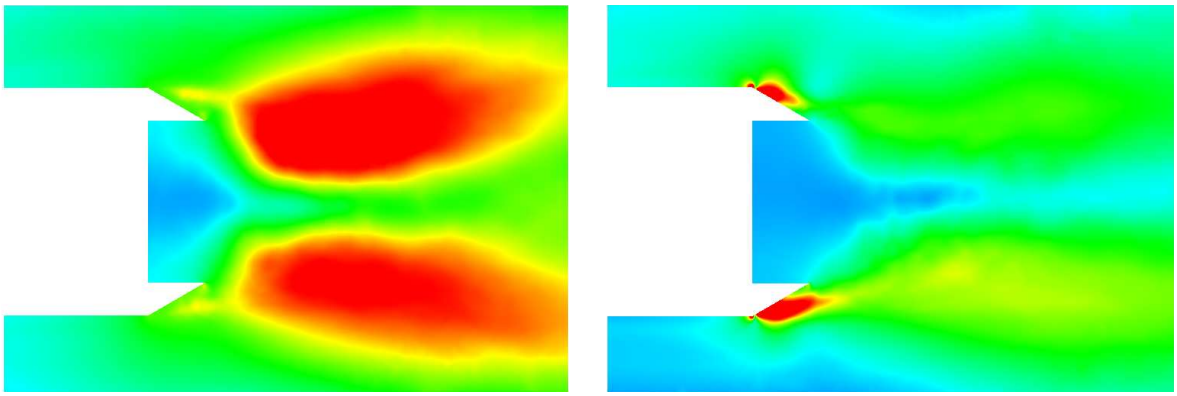

(a) AFC OFF (b) AFC ON

Figure 8: RMS of pressure contours, zoom of the wake.

at the slot location. However C_P, increases along the flap surface and on the rear end of the truck at f. We notice that the main difference in the forced and unforced cases is at surface f. The conclusion is that the pressure is here recovered by the AFC, which minimizes the pressure difference between the front and back and thus decreases the total drag of the truck.

3.4. Aerodynamic forces

Figure 10(a) plots the drag history for the forced and the unforced cases. It is clear that the forced case shows lower drag at every instant when the flow has reach fully developed conditions. We can also conclude that the drag reduction process occurs in two steps, shown in the figure; when AFC is applied, the drag initially decreases a great deal (at $t = 2\ s$) before the forced flow reaches full developed conditions. What probably happens is that the flow reattaches when momentum flux is added to and removed from the flow via the oscillating jet. Later the forcing creates the vortices that roll down the flap and keep the flow reattached over the whole flap surface, keeping the drag at a lower level than in the unforced case.

Figure 10(b) plots the power spectral density of the drag signal. We notice the vortex shed-

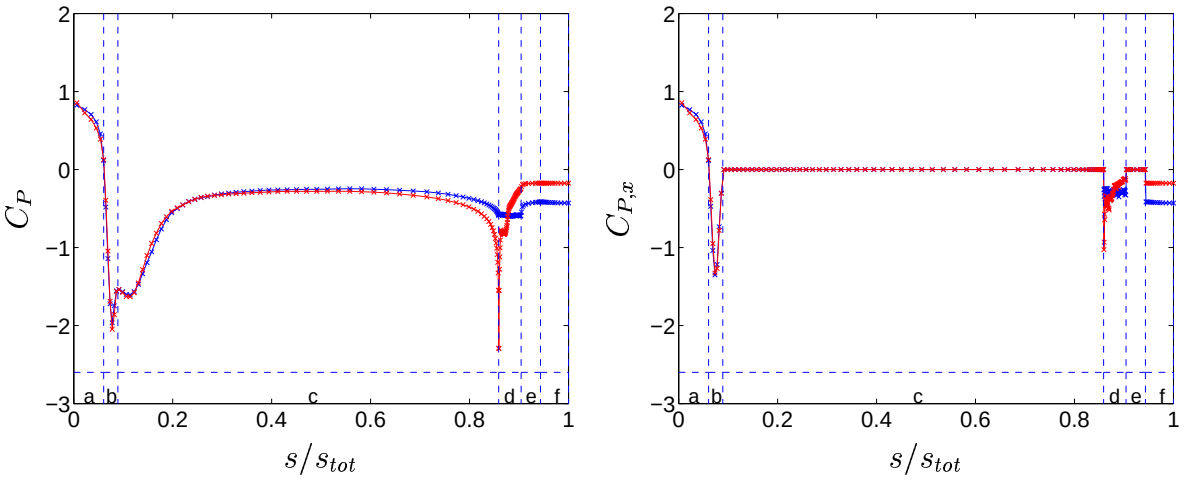

(a) Pressure coefficient.

(b) Projected pressure load in the x-direction.

Figure 9: Mean C_P and projected mean pressure load in the x-direction ($C_{P,x}$) of the upper half truck surface (symmetry). —— : AFC OFF; —— : AFC ON

ding frequency in both the unforced and forced cases with one difference. The peak of the forced case is reduced compared to the unforced case. This confirms our previous finding that the intensity of the wake is reduced by AFC. The peaks are located at frequency $0.98\ Hz$, which corresponds to a Strouhal number of $St = 0.1$. This is in good agreement with measurements made on rectangular cylinders [14]. In [14] the author measured the Strouhal number of rectangular cylinders of different B/H as a function of Reynolds number. The Strouhal number was $St = 0.12$ for $Re = 2 \cdot 10^4$ and $B/H = 4$. The present truck model has $B/H = 5$ at $Re = 2 \cdot 10^5$. We further notice the high peak at $10\ Hz$ that corresponds to the actuation frequency. The intensity of the peak is high and, for this reason, there is high RMS drag of the forced case in figure 10(a).

4. Conclusions

A novel rear end of a truck trailer is proposed, that reduces the drag by 25% or more. Several hundred large-eddy simulation cases were carried out with and without AFC. The drag reduction is comfirmed by several physical analyses of the flow comparing the instantaneous and time-averaged flow field of the unforced and the forced cases.

The instantaneous characteristics of the unforced case were found to be typical of bluff body flows, with strong global vortex shedding and reversed flow on the flaps due to a higher flap angle than the natural separation angle. The forced case has weaker vortex shedding, and small vortices were observed on the flap surface that were created by the actuation. These vortices move downstream the flap surface, creating a shear layer in the wake that prevents interaction between the naturally created shear layers on the upper and lower edges.

The unforced case has a large time-averaged low pressure region in the wake and on the flap surface, yielding a large wake structure with high intensity and a large mean drag. The flap region of the unforced case has a separated flow region, whereas the actuation forced the time-averaged flow to stay attached. There is a great suppression of the RMS of pressure in the wake owing to AFC, which decreases the level of vortex shedding in the wake and makes the wake less intensive. The RMS of pressure was increased on the flap surface with actuation, however,

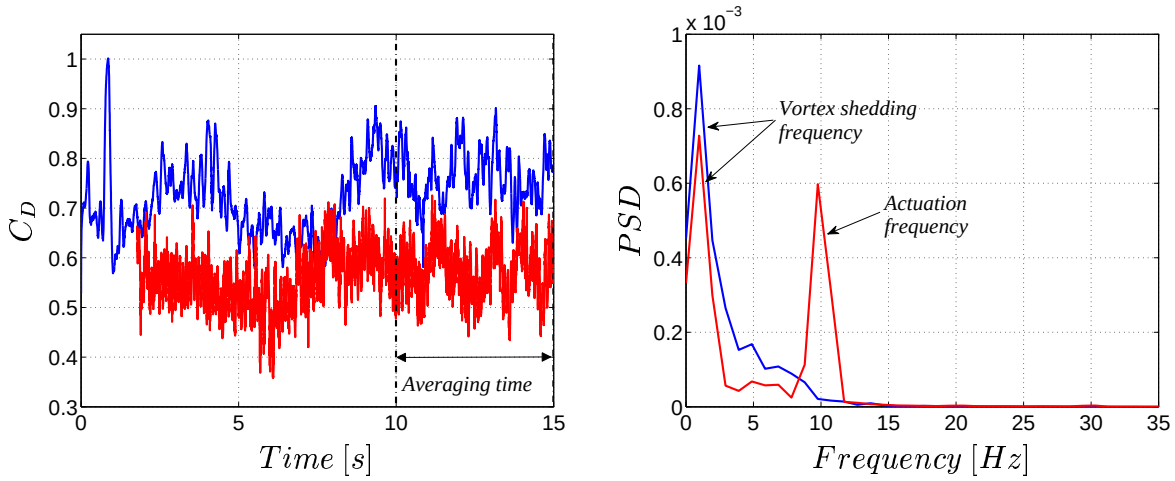

(a) Drag history

(b) Power spectral density

Figure 10: Drag history and its FFT, — : AFC OFF; — : AFC ON. $C_D^{AFC\ OFF} = 0.76$; $C_D^{AFC\ ON} = 0.57$. One time unit, w/U_∞, corresponds to $0.1\ s$.

which created a strong low pressure region at the leading edge of the flap, that makes the flow stay attached.

The low drag of the forced case is due to the increased base pressure at the rear end of the truck that was shown by the C_p analysis. The vortex shedding frequency was in good agreement with experimental results [14]. The actuation frequency was observed in the frequency analysis of the drag history, which also showed that the intensity of the vortex shedding was decreased due to AFC.

The spanwise domain and mesh resolution were also investigated in [7]. The RMS of the drag was decreased with larger size of the spanwise domain and lower mesh resolution. The flow becomes more two dimensional when the domain size is small, and the three dimensionality and the effect of AFC are much more clear in large domains. The drag reduction achieved is consistent with different spanwise domain sizes.

In [7] the actuation as periodic blowing was also investigated versus periodic blowing and suction, where the RMS of the drag was strongly reduced, and the drag reduction by the blowing and suction was not affected. The slot location was also investigated, and it was shown that the location can be moved up to $10\ cm$ from the upper edge of the flap without affecting the drag reduction achieved.

5. Acknowledgments

This work is supported by the **Swedish Agency of Innovation Systems (VINNOVA)**, **Volvo 3P**, **SKAB** and **CD-ADAPCO**. The financial support of SNIC (the Swedish National Infrastructure for Computing) for computer time at C3SE (Chalmers Centre for Computational Science and Engineering) is gratefully acknowledged.

References

1. L. Hjelm and B. Bergqvist. European truck aerodynamics - a comparison between conventional and coe truck aerodynamics and a look into future trends and possibilities. In *The Aerodynamics of Heavy Vehicles II: Trucks, Buses and Trains.*
2. M. El-Alti, P. Kjellgren, and L. Davidson. On the download alleviation for the XV-15 wing by active flow control using large-eddy simulation. In *ERCOFTAC Workshop: Direct and Large-Eddy Simulation 7*, Trieste, Italy, Sept 8-10 2008.
3. P. Kjellgren, M. El-Alti, and L. Davidson. Download alleviation of a tilt-rotor wing by active flow control strategies. In *KATnet II Conference: Key Aerodynamic Technologies*, Bremen, Germany, May 12-14 2009.
4. P. Kjellgren, A. Hassan, J. Sivasubramanian, L. Cullen, D. Cerchie, and I. Wyganski. Download alleviation for the XV-15: computations and experiments of flows around the wing. In *Biennial International Powered Lift Conference and Exhibit*, Williamsburg, Virginia, Nov 5-7 2002.
5. A. Darabi and I. Wygnanski. Active management of naturally separated flow over a solid surface. part 1. the forced reattachment process. *Journal of Fluid Mechanics*, 510:105–129, 2004.
6. M. El-Alti, V. Chernoray, P. Kjellgren, and L. Davidson. Experimental investigation of a simple synthtic-jet actuator for active flow control purposes. Internal report, Div. of Fluid Dynamics, Dept. of Applied Mechanics, Chalmers University of Technology, Göteborg, Sweden, 2009.
7. Mohammad El-Alti. Active Flow Control for Aircrafts and Heavy Vehicles. Thesis for licentiate of engineering no. 2009:011, Div. of Fluid Dynamics, Dept. of Applied Mechanics, Chalmers University of Technology, Göteborg, Sweden, 2009.
8. R. Pankajakshan, Brent Mitchell, and David L. Whitfield. Full-scale simulations of drag reduction devices for class 8 trucks. In *The Aerodynamics of Heavy Vehicles II: Trucks, Buses and Trains.*
9. J. Leuchen and K. R. Cooper. Summary of full-scale wind tunnel tests of aerodynamic drag-reducing devices for tractor-trailers. In *The Aerodynamics of Heavy Vehicles II: Trucks, Buses and Trains.*
10. A. Seifert, O. Stalnov, D. Sperber, G. Arwatz, V. Palei, S. David, I. Dayan, and I. Fono. Large trucks drag reduction using active flow control. In *The Aerodynamics of Heavy Vehicles II: Trucks, Buses and Trains.*
11. L. Henning and R. King. Drag reduction by closed-loop control of a separated flow over a bluff body with a blunt trailing edge. In *44th IEEE Conference on Decision and Control and European Control Conference ECC 2005*, pages 494–499, Seville, Spain, 2005.
12. R. J. Englar. Improved pneumatic aerodynamics for drag reduction, fuel economy, safety and stability increase for heavy vehicles. In *SAE 2005 Commercial Vehicle Engineering, Comgress and Exhibition*, SAE Paper 2005-01-3627, Chicago, Illinois, USA, 2005.
13. A. Seifert, T. Bachar, D. Koss, M. Shepshelovich, and I. Wygnanski. Oscillatory blowing: A tool to delay boundary-layer separation. *AIAA Journal*, 31(11):2052–2060, 1993.
14. A. Okajima. Strouhal numbers of rectangular cylinders. *Journal of Fluid Mechanics*, 123:379–398, 1982.